ChimeraLM: a language model enables accurate structural variant detection in whole-genome amplified long-read sequencing

Yangyang Li[1]†, Qingxiang Guo[1]†, Rendong Yang[1,2]*

[1]Department of Urology, Northwestern University Feinberg School of Medicine, 303 E Superior St, Chicago, 60611, IL, USA.
[2]Robert H. Lurie Comprehensive Cancer Center, Northwestern University Feinberg School of Medicine, 675 N St Clair St, Chicago, 60611, IL, USA.

*Corresponding author(s). E-mail(s): rendong.yang@northwestern.edu;
Contributing authors: yangyang.li@northwestern.edu; qingxiang.guo@northwestern.edu;
†These authors contributed equally to this work.

Abstract

Single-cell genomic analysis relies on whole genome amplification (WGA) to generate sufficient DNA for sequencing, yet this process introduces chimera artifacts that manifest as false-positive structural variation (SV) and compromise downstream analyses. Here we present ChimeraLM, an interpretable genomic language model (GLM) that identifies WGA-induced chimera artifacts directly from sequence information. ChimeraLM is trained on matched WGA and bulk long-read sequencing from the same sample, using bulk support to label chimeric reads as amplification-induced artifacts or genuine genomic events. To capture long-range dependencies in variable-length reads, the model integrates Hyena operators with attention pooling. Evaluated on matched WGA and bulk nanopore datasets, ChimeraLM eliminated ∼90% of chimeric reads from WGA data, restoring chimeric read proportion to near-bulk levels, whereas existing approaches achieved at most an 8% reduction. Using high-confidence SV call sets derived from matched bulk data as a reference, ChimeraLM removed 92-93% of unsupported SV calls from WGA datasets while retaining 72–92% of bulk-supported SVs. ChimeraLM further normalized SV type distributions toward bulk profiles by suppressing the characteristic inversion bias observed in unprocessed WGA data. Attention-based interpretation indicates that ChimeraLM concentrates classification evidence at chimeric junctions, demonstrating its ability to learn biologically interpretable features. ChimeraLM provides a general approach for suppressing amplification-induced artifacts, enabling more reliable single-cell SV analysis across long-read platforms.

Keywords: Whole Genome Amplification, Single Cell, Genomic Language Model, Structural Variation

Main

Single-cell and low-input genomics have transformed our ability to resolve biological heterogeneity, enabling the discovery of rare cell states and the reconstruction of clonal evolution in cancer and development [1–3]. However, the limited DNA input (on the order of picograms per cell) makes comprehensive genome-wide profiling technically challenging [4, 5]. Whole genome amplification (WGA) therefore remains a prerequisite for high-coverage sequencing [6–8], yet it introduces systematic errors that compromise genomic fidelity, particularly for structural variation (SV) detection [9–11].

A major source of error in WGA is amplification-induced chimera formation. During this process, highly processive polymerases such as phi29, which is used in multiple displacement amplification (MDA), can switch templates and join discontinuous genomic loci into a single molecule [9–13]. As a result, WGA-based sequencing often produces chimeric reads that constitute a substantial fraction of the data [9]. These artificial sequences frequently create alignment patterns that closely resemble those generated by genuine SVs, including translocations and inversions [10]. Consequently, SV callers that rely on alignment-based signals (e.g., split-read and supplementary alignments) and coverage-derived evidence often misinterpret these amplification artifacts as true rearrangements, inflating false positives and distorting SV spectra [14–22]. This problem is particularly consequential for WGA-based long-read sequencing, which is otherwise well suited for resolving complex SVs at sing-cell resolution [23, 24].

Distinguishing genuine genomic rearrangements from WGA-induced chimera artifacts remains a major computational challenge. Existing quality-control approaches typically rely on handcrafted rules or alignment-derived features, such as read orientation signatures or local coverage deviations [11, 13, 25]. However, these heuristics are often sensitive to platform- and protocol-specific variation. Moreover, they cannot capture sequence-level patterns or long-range dependencies within reads. As a result, low-input long-read sequencing remains difficult to deploy in settings where high precision is essential, including somatic mosaicism profiling [26] and validation of CRISPR off-target effects [27].

To address this challenge, we present ChimeraLM, an interpretable genomic language model (GLM) for identifying and filtering WGA-induced artifacts at the single-read level. Unlike existing approaches that rely on handcrafted rules derived from read alignments or sequence-level [11, 13, 25], ChimeraLM formulates artifact detection as a sequence-modeling task and learns discriminative features directly from raw reads [28]. Building on advances in DNA foundation models [29–32], it captures latent motifs and structural dependencies that generalize across long-read sequencing platforms provided by Oxford Nanopore Technologies (ONT). On ONT WGA datasets, ChimeraLM reduces chimeric reads by ∼90% while preserving 72–92% of bulk-supported SVs, improving SV validation rates by 8.5- to 11.0-fold and mitigating WGA-induced biases in SV type distributions. Together, ChimeraLM provides an effective and interpretable filter for WGA long-read data, enabling robust SV discovery in single-cell and low-input genomics.

Results

Overview of ChimeraLM workflow and model architecture

ChimeraLM operates as a post-alignment filtering module within the single-cell long-read sequencing pipeline (Fig. 1a). After base calling and alignment to the reference genome, the resulting read set typically contains a mixture of true chimeric reads that arise from authentic genomic rearrangements and artificial chimeras introduced during WGA. ChimeraLM evaluates all reads with chimeric alignments before variant calling. For each read, the model determines whether the observed chimera reflects a genuine genomic event or a WGA-induced artifact. This binary classification enables selective removal of artificial chimeric reads while preserving true rearrangements, which improves the accuracy and sensitivity of downstream SV analyses.

To construct a robust supervised training set, we generated WGA long-read sequencing data from the human prostate cancer cell line PC3 using the ONT PromethION platform. For ground-truth calibration, we acquired three matched bulk long-read datasets from unamplified genomic DNA across diverse technologies: ONT PromethION, ONT MinION, and Pacific Biosciences (PacBio) Sequel II. Leveraging these references, we established a bulk-supported labeling framework by cross-referencing each WGA chimeric read against the chimeric alignment structures identified in the unamplified bulk data (Methods; Fig. 1b; Extended Data Fig. 1a). Under this classification scheme, WGA reads with alignment architectures corroborated by bulk evidence were labeled as genuine genomic events, while those lacking bulk support were classified as WGA-induced artifacts. To evaluate the model's ability to generalize across sequencing hardware, we generated an independent WGA dataset on the MinION platform, which was reserved exclusively for testing (Extended Data Fig. 1a).

This labeling procedure classified 12,963,576 chimeric reads from the WGA PromethION dataset into two groups (genuine events and WGA-induced artifacts) based on bulk support (Extended Data Fig. 1b). Among these, 12,670,396 reads (97.7%) showed no matching alignment structures in any bulk dataset and were labeled as WGA-induced artifacts. The remaining 293,180 reads (2.3%) had matching structures in at least one bulk dataset, indicating they represent genuine genomic events rather than amplification artifacts, and were labeled as genuine chimeric reads. To construct a balanced training dataset, we retained all 293,180 genuine chimeric reads and randomly subsampled an equal number of WGA-induced artifacts. We further added 178,748 chimeric reads sampled from the bulk datasets to the genuine-event set, expanding the diversity of bulk-supported chimeric alignment structures used for training. The final

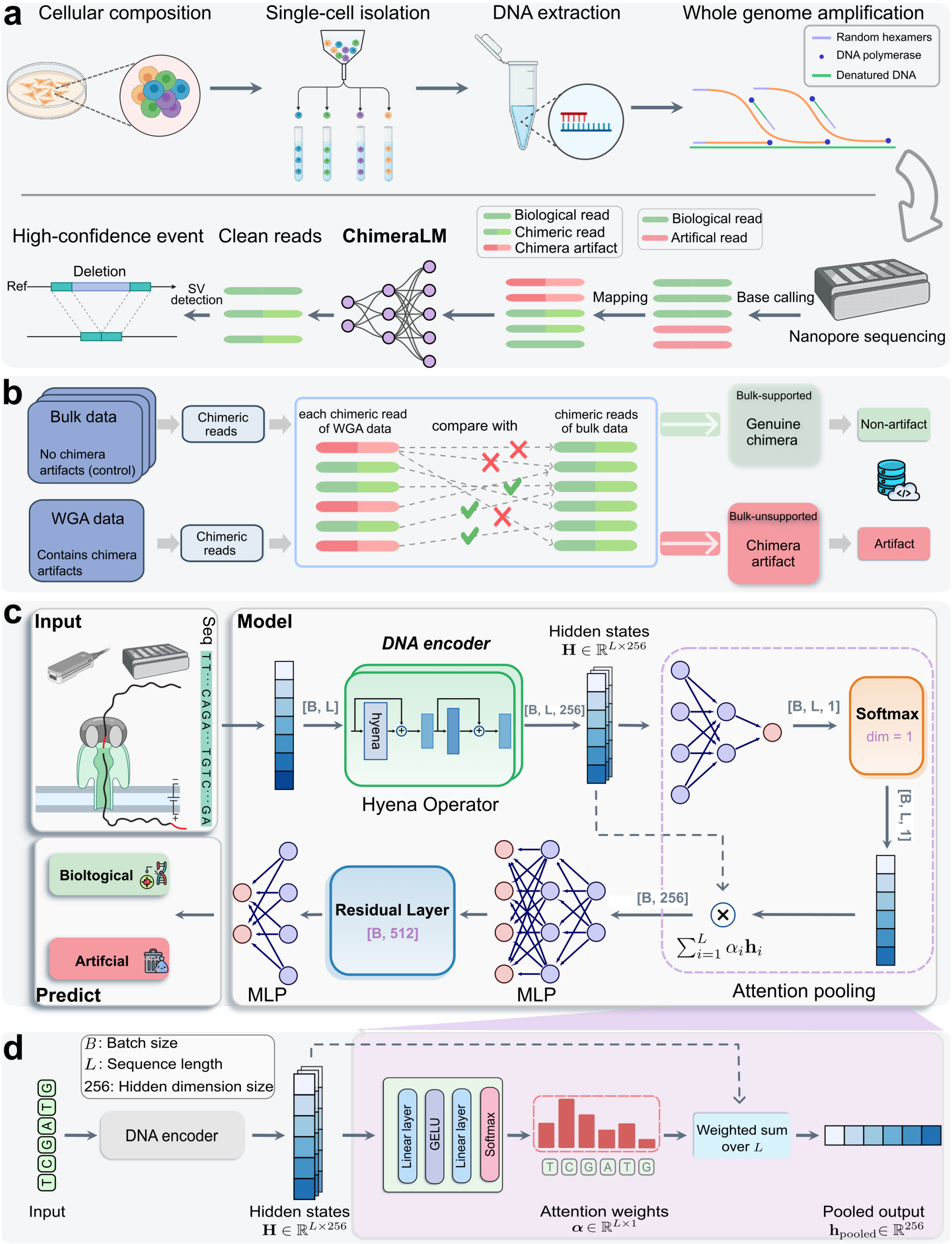

Fig. 1 ChimeraLM workflow and architecture for detecting WGA artifacts. (a) Single-cell genomic workflow and ChimeraLM integration. Single cells are isolated, followed by DNA extraction and WGA. During amplification, WGA-induced chimeric artifacts (red) are generated alongside genuine chimeric reads (green). After base calling and mapping, ChimeraLM classifies reads with chimeric alignments as genuine events or WGA-induced artifacts, enabling downstream SV detection on filtered data. **(b)** Bulk-supported label generation. Chimeric reads from WGA data are compared against bulk sequencing from the same cell line. Reads with bulk-supported alignment structures are labeled as genuine events (green); reads with no bulk match are labeled as WGA-induced artifacts (red). **(c)** ChimeraLM architecture. Input DNA sequences (batch size B, sequence length L) are tokenized at single-nucleotide resolution and encoded into hidden states $\mathbf{H} \in \mathbb{R}^{L\times 256}$ through DNA encoder (HyenaDNA [29]). Hyena operators capture long-range dependencies. Attention pooling aggregates position-specific features, and multilayer perceptron (MLP) layers with residual connections process pooled representations for binary classification of genuine events and WGA-induced artifacts. **(d)** Attention pooling mechanism. Attention weights $\boldsymbol{\alpha} \in \mathbb{R}^{L\times 1}$ are computed through linear layers with GELU activation and softmax normalization, assigning importance scores to each position. The weighted sum produces a fixed-dimensional representation $\mathbf{h}_{\text{pooled}} \in \mathbb{R}^{256}$. Created with BioRender.com.

labeled dataset comprised 765,108 reads and was split into training (70%), validation (20%), and test (10%) sets using stratified sampling (Extended Data Fig. 1a).

To model these labeled reads, ChimeraLM needs to process long, variable-length DNA sequences at single-nucleotide resolution (Fig. 1c). We therefore built ChimeraLM on HyenaDNA [29], a genomic foundation model pre-trained on diverse DNA sequences. Each read is tokenized at nucleotide resolution and encoded by Hyena operators [33], which capture long-range sequence context without splitting the input. The encoder produces a sequence of hidden states across the full read. To obtain a fixed-length representation for classification, ChimeraLM uses an attention-pooling module that learns position-specific weights and computes a weighted sum over the hidden states (Fig. 1d). The pooled representation is then passed through residual MLP blocks, and a final softmax outputs the probability that a read reflects a genuine event versus a WGA-induced artifact.

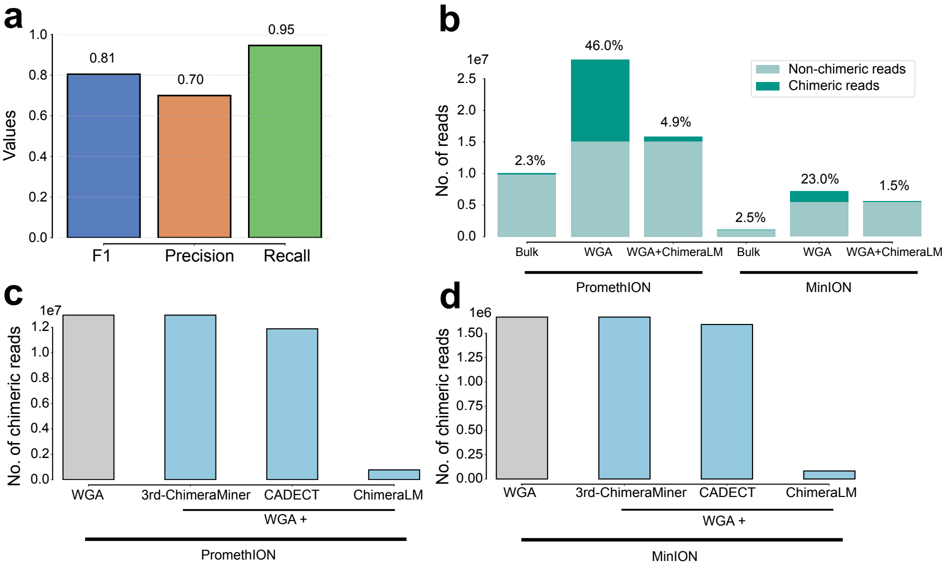

Fig. 2 ChimeraLM accurately identifies and removes WGA-induced chimeric artifacts. **(a)** Classification performance on held-out test data. ChimeraLM achieves recall of 0.95, precision of 0.70, and F1 score of 0.81. **(b)** Chimeric read reduction across sequencing platforms. Stacked bars show proportions of chimeric (dark teal) and non-chimeric (light teal) reads in bulk, WGA, and ChimeraLM-filtered samples. ChimeraLM reduces chimeric read frequencies from 46.0% to 4.9% (PromethION) and from 23.0% to 1.5% (MinION), approaching bulk levels (2.3% and 2.5%, respectively). **(c,d)** Benchmarking against existing methods on PromethION (c) and MinION (d). The gray bar indicates the total number of chimeric read on unfiltered WGA data. The blue bar represents the total number of chimeric reads remaining after filtering by each method. ChimeraLM achieves approximately 90% reduction in chimeric reads on both platforms, while 3rd-ChimeraMiner shows no detectable reduction and CADECT shows 8.3% and 4.6% reduction on PromethION and MinION, respectively. SACRA failed to complete due to memory exhaustion (> 500 GB RAM required).

ChimeraLM achieves high accuracy and reduces artifacts to near-bulk levels across platforms

We first benchmarked ChimeraLM using the held-out test split (10%) derived from the bulk-supported labeled dataset (Extended Data Fig. 1a). This test set consists of chimeric reads labeled as genuine events or WGA-induced artifacts based on whether their chimeric alignment structures are supported by matched bulk sequencing. ChimeraLM achieved an F1 score of 0.81, with 0.95 recall and 0.70 precision (Fig. 2a). The high recall indicates that most WGA-induced artifacts are correctly identified for removal, which is important for limiting downstream false-positive SV calls, while the precision confirms that most reads flagged as artifacts are true amplification-induced chimeras rather than genuine genomic events.

We next examined whether applying ChimeraLM filtering would restore chimeric read rates in full PC3 WGA datasets toward the levels observed in bulk sequencing across both PromethION and MinION platforms (Fig. 2b). Bulk sequencing established low baseline chimeric read rates of 2.3% (PromethION) and 2.5% (MinION). In contrast, WGA increased the chimeric read fraction to 46.0% and 23.0%, respectively. After ChimeraLM filtering, chimeric content dropped to 4.9% on PromethION and 1.5% on MinION, corresponding to 10- to 15-fold reductions, while retaining 15.8 million and 5.6 million reads. These post-filtering rates approach the corresponding bulk baselines, indicating effective removal of WGA-induced artifacts while preserving genuine signal.

We compared ChimeraLM against SACRA [25], 3rd-ChimeraMiner [13], and CADECT [11], existing tools for detecting amplification-induced chimeras (Fig. 2c,d). ChimeraLM reduced chimeric reads by ∼90% on both platforms, outperforming CADECT (8.3% and 4.6% reduction on PromethION and MinION, respectively), while 3rd-ChimeraMiner showed no detectable reduction. SACRA could not be evaluated due to out-of-memory errors even with 500 GB RAM.

The MinION results further provide an independent test of model generalization, as this MinION WGA dataset was not used during training. ChimeraLM was trained exclusively on PromethION WGA data, yet achieved comparable chimeric read reduction on MinION. This cross-platform generalization indicates that ChimeraLM captures sequence-level features intrinsic to WGA-induced artifacts rather than platform-specific signatures, supporting its potential applicability to additional long-read and potentially short-read sequencing technologies.

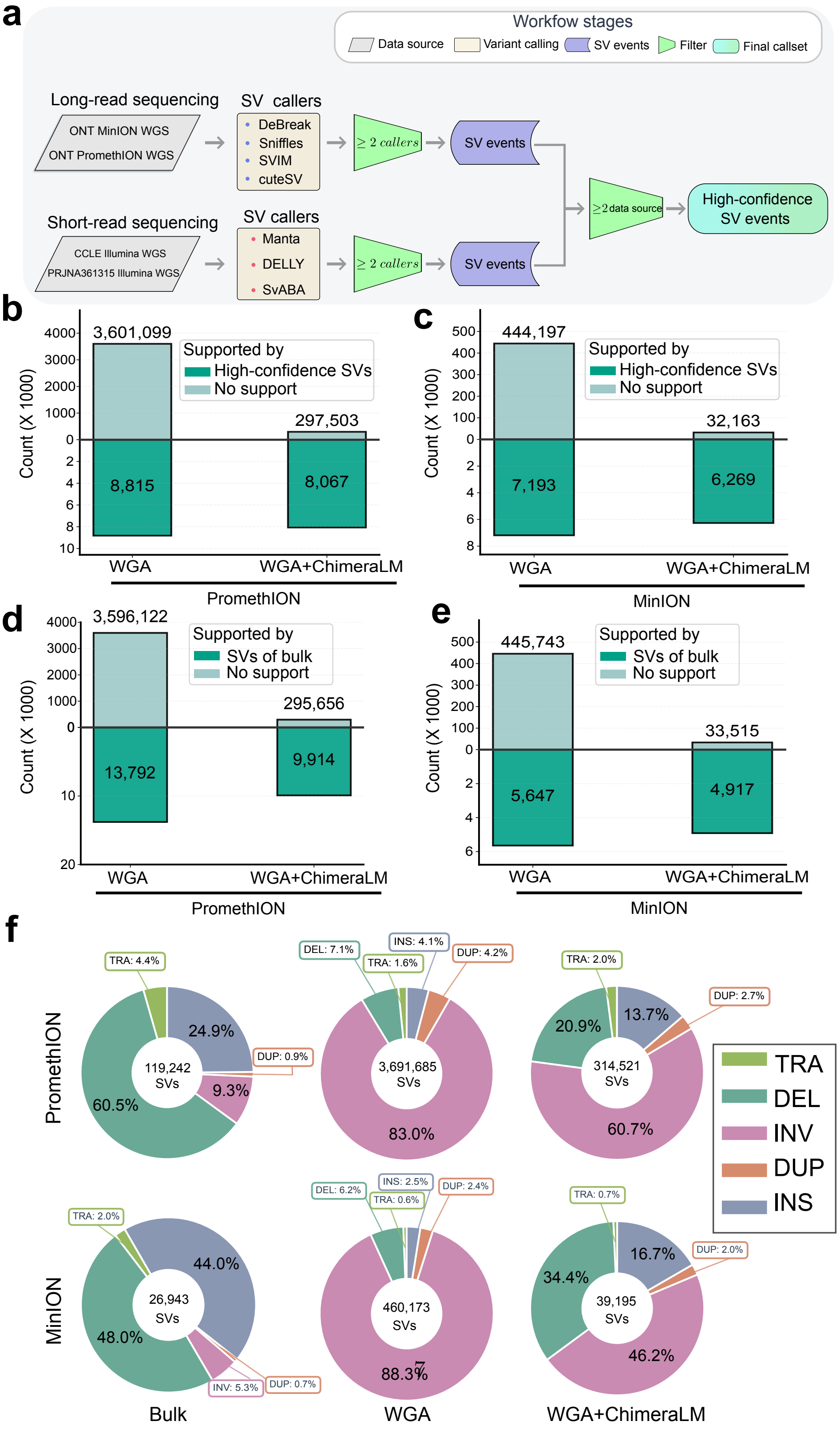

Fig. 3 ChimeraLM improves structural variant detection accuracy. (a) Construction of a high-confidence SV reference dataset from bulk PC3 sequencing. Four bulk datasets were integrated: ONT MinION Mk1C, ONT PromethION P2, the CCLE Illumina whole genome sequencing (WGS) dataset, and the PRJNA361315 Illumina WGS dataset. SVs were called independently within each dataset using multiple callers, and events supported by ≥2 callers per dataset were retained. SVs were then compared across datasets, and events observed in ≥2 of the four bulk datasets were designated as gold-standard SVs. **(b,c)** SV validation against the gold-standard reference for PromethION (b) and MinION (c). Bars show SV calls supported by the gold standard (dark teal) or unsupported (light teal). **(d,e)** SV validation against platform-matched long-read bulk sequencing for PromethION (d) and MinION (e), capturing true long-read SVs that may not be represented in the multi-platform reference. Bars show SV calls supported by the platform-matched long-read bulk data (dark teal) or unsupported (light teal). **(f)** Distribution of SV types for PromethION and MinION datasets across bulk samples, unfiltered WGA, and WGA with ChimeraLM filtering. Unfiltered WGA exhibits an excess of inversion (INV) events, which is substantially reduced following ChimeraLM filtering. Other SV classes, including translocation (TRA), deletion (DEL), duplication (DUP), and insertion (INS), are also shown.

ChimeraLM reduces unsupported structural variant calls

Accurate SV detection from single cells is essential for characterizing genomic diversity and disease mechanisms. However, WGA-induced chimeric artifacts can be misinterpreted as genuine SVs, potentially leading to incorrect biological inferences. To assess the impact of ChimeraLM on SV calling, we compared SV callsets generated from unfiltered WGA reads with those obtained after applying ChimeraLM filtering (WGA + ChimeraLM). Both callsets were evaluated against two complementary bulk-derived references: (i) a stringent gold-standard SV set derived from bulk PC3 DNA through cross-dataset consensus, and (ii) platform-matched long-read bulk SV callsets used as platform-specific references.

We first constructed a high-confidence gold-standard SV set from bulk PC3 DNA by integrating four independent sequencing datasets: ONT PromethION, ONT MinION, and two Illumina short-read WGS datasets from the Cancer Cell Line Encyclopedia (CCLE Illumina WGS [34]) and from a previously published study (PRJNA361315 Illumina WGS [35]) (Fig. 3a; Extended Data Table 1). SVs were called separately within each dataset using multiple SV callers. Events supported by at least two callers within a dataset were retained, and only SVs observed in at least two of the four datasets were designated as gold-standard events.

Relative to this stringent gold standard, unfiltered WGA produced a large number of unsupported SVs. On PromethION, WGA yielded 3,601,099 SV calls, of which only 8,815 (0.24%) overlapped gold-standard events. After ChimeraLM filtering, total calls decreased to 305,570 (a 91.5% reduction) while retaining 8,067 gold-standard events (91.5% retention), increasing the validation rate to 2.64% (11-fold) (Fig. 3b). On MinION, total calls decreased from 451,390 to 38,432 (a 91.5% reduction), while gold-standard-supported events decreased from 7,193 to 6,269, corresponding to 87.2% retention. The validation rate increased from 1.59% to 16.3% (10-fold) (Fig. 3c).

Because the gold standard is intentionally stringent and may exclude true SVs detectable only in long-read data, we next performed platform-matched validation using long-read bulk sequencing from the same platform (Fig. 3d,e). This analysis provides a platform-specific estimate of recall and reduces bias introduced by the strict gold-standard definition. ChimeraLM increased validation rates from 0.38% to 3.24% on PromethION (8.5-fold) and from 1.25% to 12.79% on MinION (10-fold), while retaining 71.9% and 87.1% of bulk-supported events, respectively. Together, these results show that ChimeraLM removes the vast majority of unsupported SV calls while preserving the majority of bulk-supported variants across platforms.

ChimeraLM mitigates WGA-induced SV type biases

Amplification artifacts can profoundly distort the apparent spectrum of SVs, complicating biological interpretation. To quantify these effects, we compared SV-type compositions across bulk, unfiltered WGA, and ChimeraLM-filtered datasets generated on both ONT PromethION and MinION platforms (Fig. 3f). Bulk datasets displayed SV profiles dominated by deletions and insertions, whereas WGA datasets exhibited a striking inflation of inversions, reaching 83.0% on PromethION and 88.3% on MinION. This inversion-heavy signature mirrors previous observations from single-cell long-read sequencing using PacBio and droplet-based MDA [22], suggesting that many of these events arise from amplification-induced chimeras rather than genuine genomic rearrangements.

To directly assess which SV types are preferentially associated with amplification artifacts, we examined SV calls supported exclusively by reads classified as WGA-derived chimeras. These artifact-supported events were overwhelmingly enriched for inversions, comprising 88.4% on PromethION and 92.4% on MinION (Extended Data Fig. 2). Smaller fractions of deletions, duplications, and insertions were also present, indicating that WGA artifacts inflate not only inversion calls but generate false positives across multiple SV categories.

Applying ChimeraLM substantially reduced these biases. The inversion fraction decreased from 83.0% to 60.7% on PromethION and from 88.3% to 46.2% on MinION, while the relative abundance of deletions and insertions increased toward bulk-like levels (Fig. 3f). By selectively removing artifact-supported events, ChimeraLM suppresses the dominant inversion inflation and reduces spurious calls across SV types, shifting SV-type distributions toward bulk profiles and improving the accuracy and interpretability of single-cell SV analyses [22].

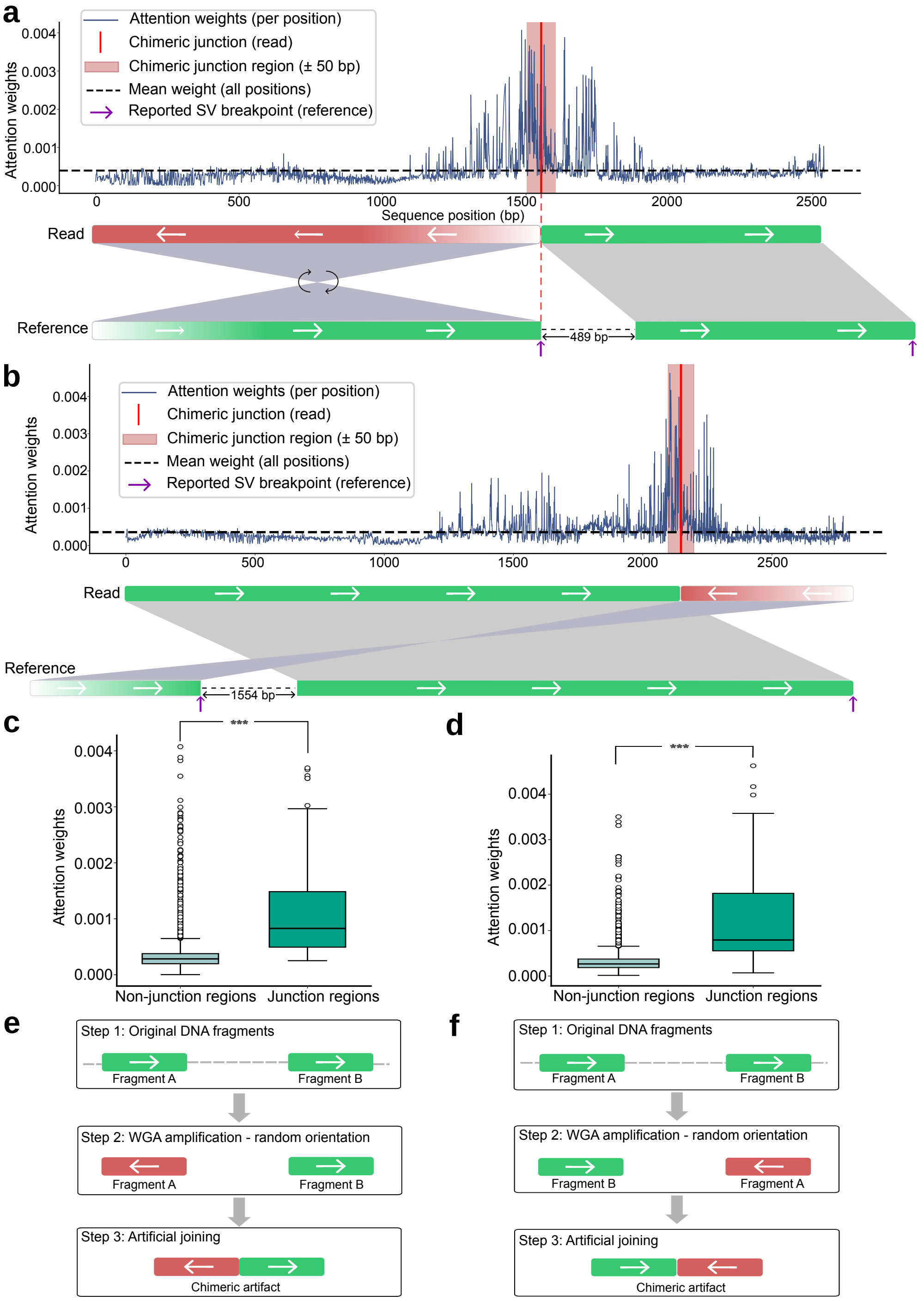

Fig. 4 ChimeraLM attention weights are enriched at chimeric junction regions. (a,b) Attention weight profiles for two representative chimeric reads exhibiting distinct junction configurations. Upper panels show per-position attention weights (blue) with the mean attention across the read indicated by a dashed line. Red vertical lines mark inferred chimeric junction positions, and pink shading denotes the junction-centered region (±50 bp). Lower panels display read-level alignments, highlighting orientation transitions at the junctions (green, forward orientation; red, reverse-complemented orientation). **(c,d)** Quantitative comparison of attention weights between junction and non-junction regions. Junction-centered windows show significantly elevated attention weights relative to non-junction regions ($P = 5.3 \times 10^{-14}$ and $P = 6.8 \times 10^{-15}$; Wilcoxon rank-sum test). **(e,f)** Schematic illustration of WGA-induced chimera formation. During amplification, DNA fragments originating from distant genomic loci can be amplified in either orientation, joining them into a single molecule with discordant orientations, producing inversion-like alignment signatures. The two examples illustrate forward-to-reverse and reverse-to-forward orientation transitions.

Attention visualization reveals interpretable classification features

We examined whether ChimeraLM's attention weights provide an interpretable signal by focusing on mechanistically relevant regions of chimeric reads, particularly the junctions during WGA (Fig. 4). We inspected two representative chimeric reads exhibiting distinct junction configurations (Fig. 4a,b). In both cases, attention remained relatively flat across most positions but formed sharp, concentrated peaks at the inferred junction regions. These peaks aligned with the read-level breakpoint separating two genomic loci and coincided with an orientation transition between adjacent alignment segments.

To quantify this effect, we compared attention weights within junction-centered windows (±50 bp) against weights from non-junction regions (Fig. 4c,d). Junction windows showed significantly higher attention weights (Wilcoxon rank-sum test, $P = 5.3\times10^{-14}$ and $P = 6.8\times10^{-15}$), indicating that ChimeraLM preferentially emphasizes sequence context proximal to chimeric junctions.

This attention enrichment is consistent with the expected structure of WGA-induced chimeras (Fig. 4e,f): DNA fragments from distant loci can be amplified in either orientation and subsequently joined, generating junctions with discordant orientations. Together, these results suggest that ChimeraLM's attention peaks provide a mechanistically interpretable signal that concentrates classification evidence to junction-proximal sequence positions within individual reads.

Discussion

WGA enables genomic analysis from single cells and other low-input samples, but it also introduces chimeric artifacts that compromise SV detection. ChimeraLM addresses this challenge by classifying chimeric reads as genuine events or WGA-induced artifacts directly from read information, and removing artifacts before variant calling, rather than attempting to correct artifact-driven calls post hoc. Across ONT platforms, ChimeraLM improved data quality at the read and variant levels: it reduced chimeric reads by ∼90% while retaining 72–92% of bulk-supported SVs, and it increased the ratio of supported SV calls by 8.5–11.0-fold. Notably, performance generalized from PromethION (used for training) to MinION without platform-specific retraining, suggesting that ChimeraLM captures properties shared by WGA-induced artifacts rather than instrument-specific signatures.

In comparison, existing methods showed limited effectiveness on our ONT WGA datasets. Two tools originally developed and primarily evaluated on PacBio data (SACRA and 3rd-ChimeraMiner) [13, 25] either failed to complete under our evaluation setting (SACRA, $>$ 500 GB RAM) or showed no detectable reduction (3rd-ChimeraMiner), highlighting poor cross-platform generalization. CADECT [11], which was designed for ONT data, achieved only 8.3% and 4.6% reduction on PromethION and MinION, respectively. CADECT detects concatemers via sliding-window self-alignment, an effective strategy for repeat-like structures with internal sequence similarity, but it is not designed to capture the broader diversity of WGA-induced chimeras. Together, these comparisons suggest that rule-based or subtype-specific heuristics do not comprehensively address amplification-induced chimeras and motivate learning-based models that can extract discriminative sequence signatures without imposing predefined structural assumptions.

ChimeraLM also illustrates the value of deep learning for quality-control problems where conventional alignment- and coverage-derived criteria provide limited resolution. [11, 13, 25, 28]. By learning directly from sequence, ChimeraLM discovers subtle compositional and structural features that separate genuine events from amplification artifacts. The model also offers interpretability through attention visualization: attention weights concentrate at junction regions where template switching joins discordant loci, validating the biological relevance of the learned features. These methodological advances have direct implications for single-cell genomics, where high false-positive rates in WGA data have constrained robust characterization of chromosomal instability, clonal evolution, and SV burden [20, 22, 36]. By improving the signal-to-noise ratio and clarifying SV-type spectra that are otherwise distorted by amplification artifacts, ChimeraLM enables more confident identification of genuine SVs, supporting studies of cancer evolution, developmental biology, and somatic mosaicism where single-cell resolution is essential [26, 27].

Several limitations warrant consideration. First, the current model processes reads independently; integrating contextual features such as coverage or phasing information may further enhance accuracy. Second, regarding computational resources, while central processing unit (CPU) inference is feasible, graphics processing unit (GPU) acceleration is recommended for processing large-scale datasets. Finally, future work should extend validation to diverse cell types, sequencing platforms (e.g., PacBio HiFi), and alternative WGA protocols, including multiple annealing and looping-based amplification cycles (MALBAC) [37], linear amplification via transposon insertion (LIANTI) [5], primary template-directed amplification (PTA) [19], and droplet-based MDA (dMDA) [38]. While the sequence-based approach suggests broad applicability, systematic validation across amplification chemistries is needed to assess generalization limits and optimize performance for specific protocols.

More broadly, ChimeraLM illustrates the potential of GLMs for data quality control. As long-context architectures continue to advance [29], extending the model's context window to handle megabase-scale inputs could enable artifact detection in more complex genomic structures. This framework could extend to other amplification-dependent technologies, such as cell-free DNA analysis, ancient DNA studies, and low-biomass metagenomics. Furthermore, attention-based interpretability opens opportunities for studying template-switching dynamics, potentially guiding the development of improved amplification protocols. In summary, ChimeraLM provides a practical and interpretable framework for enhancing long-read single-cell genomic fidelity, ensuring that downstream biological insights are derived from genuine SVs rather than technical artifacts.

Methods

Cell culture, single-clone preparation, and nanopore sequencing

Cell culture and single-clone establishment

PC3 prostate cancer cells (ATCC® CRL-1435™) were cultured in RPMI-1640 medium supplemented with 10% fetal bovine serum and 1% penicillin–streptomycin at 37 °C with 5% CO_2. To minimize biological heterogeneity, a monoclonal population was established by serial dilution in 96-well plates, ensuring that each culture originated from a single cell. Mycoplasma contamination was routinely tested and confirmed negative prior to DNA extraction.

DNA extraction and whole-genome amplification

From the monoclonal population, two types of DNA samples were prepared: a bulk (non-amplified) control and ten single-cell MDA-amplified genomes. Bulk high-molecular-weight DNA was extracted using the Monarch® HMW DNA Extraction Kit for Cells & Blood (New England Biolabs). Individual cells were isolated using 1CellDish-60 mm (iBiochips) and amplified using the REPLI-g Advanced DNA Single Cell Kit (Qiagen) following the manufacturer's protocol. DNA concentration and fragment integrity were assessed with a Qubit 4 fluorometer and Agilent TapeStation (DNA 1000/5000 ScreenTape). Only samples meeting quality standards were used for library construction.

Nanopore library preparation and sequencing

Libraries were prepared using the ONT Ligation Sequencing Kit V14 (SQK-LSK114) and sequenced on MinION Mk1C or PromethION P2 Solo devices with R10.4.1 flow cells following the manufacturer's genomic DNA workflow. Because all single-cell samples originated from the same monoclonal lineage, differences between amplified and bulk datasets primarily reflect MDA-induced artifacts rather than biological variation.

Basecalling and read processing

POD5 files were basecalled using Dorado v0.5.0 with the high-accuracy model `dna_r10.4.1_e8.2_400bps_hac@v4.3.0` [39]. Reads with mean quality < 10 or length < 500 bp were removed. Adapters and concatemers were trimmed using Cutadapt v4.0 [40] in a two-pass, error-tolerant procedure. Filtered reads were aligned to the GRCh38.p13 reference genome using minimap2 v2.26 (`map-ont` preset) [41]. BAM files were sorted and indexed using SAMtools v1.16 [42]. Read-length and mapping statistics were computed using NanoPlot v1.46.1 [43]. All samples were processed using identical parameters.

Chimeric read identification

Chimeric reads were identified from BAM files using supplementary alignment (SA) tags. Reads were classified as chimeric if they (i) were mapped, (ii) contained an SA tag, (iii) were primary alignments (not secondary), and (iv) were not supplementary alignments themselves. This definition counts each chimeric read once using its primary alignment while excluding secondary/supplementary records, thereby avoiding double-counting and reducing ambiguity from low-confidence alignments. Reads lacking SA tags were classified as non-chimeric.

Training data construction

Data generation and sources

To construct the training dataset, we generated WGA and bulk sequencing data from PC3 cells. The WGA sample was amplified and sequenced on the PromethION P2 platform (ONT), while three independent bulk datasets were produced from non-amplified genomic DNA: bulk PromethION P2, bulk MinION Mk1c (ONT), and bulk PacBio. These bulk datasets represent authentic biological sequences free from amplification-induced artifacts. In contrast, WGA sequencing includes both genuine genomic reads and artificial chimeras introduced during the amplification process.

Ground truth annotation and class definition

Ground truth labels were established by systematically comparing chimeric reads from the WGA PromethION P2 dataset against those from the three bulk datasets. For each WGA chimeric read, all alignment segments—defined by their genomic start and end coordinates—were compared to the corresponding segments of bulk chimeric reads. A WGA read was labeled as biological if every segment matched at least one bulk chimeric read within a 1 kb positional tolerance, indicating that the structural configuration is also present in non-amplified DNA. Reads lacking any matching pattern across all bulk datasets were labeled as artificial chimeras, presumed to arise from the amplification process. Additional chimeric reads were randomly sampled from the bulk datasets and labeled as biological, as these reads originate from genuine genomic rearrangements such as true SVs. The final labeled dataset combined the annotated WGA PromethION P2 reads with the subsampled bulk chimeric reads and was subsequently partitioned into training, validation, and test sets as described below.

Dataset partitioning and cross-platform validation

The combined labeled dataset, derived from WGA PromethION P2 and bulk sequencing data, was divided into training (70%), validation (20%), and test (10%) sets using stratified random sampling. These subsets were used respectively for model training, hyperparameter tuning, and performance evaluation on data from the same sequencing platform.

To evaluate cross-platform generalization, the complete WGA MinION Mk1c dataset was reserved. This dataset, generated on a different nanopore platform, was never used during model training or internal testing. This two-level evaluation design allowed us to test whether ChimeraLM captures general sequence features of amplification-induced chimeras rather than platform-specific artifacts.

Model architecture

DNA encoder

ChimeraLM employs the pre-trained HyenaDNA model [29] as its DNA encoder. This model was pre-trained on large-scale genomic data and provides robust sequence representations. DNA sequences are tokenized at single-nucleotide resolution, with each base (A, C, G, T, N) mapped to a unique integer token (7, 8, 9, 10, 11, respectively). Special tokens include [CLS]=0, [PAD]=4, and others for sequence processing. Input sequences are truncated at 32,768 bp or padded to enable batch processing.

For a tokenized input sequence $\mathbf{x} \in \mathbb{Z}^L$, the HyenaDNA generates contextualized hidden representations:

$$\mathbf{H} = \text{HyenaDNA}(\mathbf{x}) \in \mathbb{R}^{L \times 256}$$

where $\mathbf{H} = (\mathbf{h}_1, \mathbf{h}_2, \ldots, \mathbf{h}_L)$ represents position-wise hidden states with dimension 256. The Hyena operators [33] efficiently capture both local sequence motifs and long-range dependencies essential for distinguishing biological sequences from chimeric artifacts.

Attention pooling

To aggregate variable-length sequence representations into fixed-size vectors, ChimeraLM implements attention-based pooling. For hidden states $\mathbf{H} \in \mathbb{R}^{L \times 256}$, attention weights are computed through a two-layer network:

$$\begin{aligned}
\mathbf{e} &= \text{GELU}(\text{Linear}_{256 \to 256}(\mathbf{H})) \in \mathbb{R}^{L \times 256} \\
\mathbf{s} &= \text{Linear}_{256 \to 1}(\mathbf{e}) \in \mathbb{R}^{L \times 1} \\
\boldsymbol{\alpha} &= \text{softmax}(\mathbf{s}) \in \mathbb{R}^{L \times 1}
\end{aligned}$$

The pooled representation is the weighted sum of hidden states:

$$\mathbf{h}_{\text{pooled}} = \sum_{i=1}^{L} \alpha_i \mathbf{h}_i \in \mathbb{R}^{256}$$

This mechanism assigns learned importance weights to each sequence position, enabling the model to focus on informative regions while accommodating natural variability in read lengths.

Classification head

The pooled representation is processed through a MLP with residual connections. The first layer expands dimensionality:

$$\mathbf{f}_1 = \text{Dropout}_{0.1}(\text{GELU}(\text{Linear}_{256 \to 512}(\mathbf{h}_{\text{pooled}}))) \in \mathbb{R}^{512}$$

Subsequent residual blocks with input $\mathbf{f}_{\text{in}} \in \mathbb{R}^{512}$ compute:

$$\mathbf{f}_{\text{out}} = \text{Dropout}_{0.1}(\text{Linear}_{512 \to 512}(\text{GELU}(\text{Linear}_{512 \to 512}(\mathbf{f}_{\text{in}})))) + \mathbf{f}_{\text{in}}$$

where the skip connection enables stable gradient flow during training. The final layer produces binary classification logits:

$$\mathbf{z} = [z_0, z_1] = \text{Linear}_{512\to 2}(\mathbf{f}_{\text{final}}) \in \mathbb{R}^2$$

where z_0 and z_1 represent logits for biological and artificial chimeric classes, respectively. During inference, the predicted class is $\hat{y} = \text{argmax}_{i\in\{0,1\}} z_i$.

Model summary

The complete ChimeraLM pipeline processes DNA sequences through: (1) single-nucleotide tokenization, (2) HyenaDNA backbone encoding to generate contextualized representations, (3) attention pooling to aggregate position-specific features, (4) MLP layers with residual connections to learn classification features, and (5) binary classification output. The entire model with ∼4.2M trainable parameters is trained end-to-end using labeled data.

Model training and optimization

Training configuration

ChimeraLM was trained using PyTorch [44] and PyTorch Lightning [45] frameworks. Input sequences were tokenized using the tokenizer with maximum sequence length of 32,768 bp. Sequences longer than this threshold were truncated; shorter sequences were padded to enable batch processing. Training employed mixed-precision computation (bf16) to accelerate training while maintaining numerical stability.

Optimization procedure

We used the AdamW optimizer [46] with learning rate $\eta = 1 \times 10^{-4}$ and weight decay $\lambda = 0.01$. AdamW implements adaptive learning rates with decoupled weight decay, combining the benefits of Adam optimization with proper L2 regularization. A ReduceLROnPlateau scheduler dynamically adjusted the learning rate based on validation loss, reducing it by a factor of 0.1 when no improvement occurred for 10 consecutive epochs. Early stopping with patience of 10 epochs prevented overfitting by terminating training when validation performance plateaued. A fixed random seed (12345) ensured reproducibility across training runs.

The training objective used cross-entropy loss for binary classification. For a training example with class label $y \in \{0, 1\}$ and model logits $\mathbf{z} = [z_0, z_1]$, the loss is:

$$\mathcal{L}(\mathbf{z}, y) = -\log\left(\frac{\exp(z_y)}{\exp(z_0) + \exp(z_1)}\right) = -z_y + \log(\exp(z_0) + \exp(z_1))$$

where z_0 and z_1 represent logits for biological and artificial chimeric classes, respectively.

Training implementation

Training used batch size of 16 sequences with 30 parallel data loading workers. GPU acceleration was employed for efficient processing, with training typically requiring

55 hours. Model checkpointing saved the best-performing model based on validation metrics. Configuration management used Hydra [47] to enable reproducible experimentation.

Model evaluation

Performance was monitored using precision, recall, and F1 score on the validation set after each epoch:

$$\text{Precision} = \frac{\text{TP}}{\text{TP} + \text{FP}}, \quad \text{Recall} = \frac{\text{TP}}{\text{TP} + \text{FN}}$$
$$\text{F1} = \frac{2 \times \text{Precision} \times \text{Recall}}{\text{Precision} + \text{Recall}}$$

where TP (true positives) are chimeric reads correctly classified as artificial, TN (true negatives) are biological reads correctly classified as biological, FP (false positives) are biological reads misclassified as artificial, and FN (false negatives) are artificial reads misclassified as biological. Final model selection was based on best validation performance as determined by early stopping.

Model inference and application

Inference pipeline

To apply ChimeraLM to new WGA sequencing data, the model takes a BAM file as input. Chimeric reads are identified using SA tags and filtered to exclude unmapped, secondary, or supplementary alignments. Each chimeric read sequence is tokenized using the tokenizer (maximum length 32,768 bp, with truncation or padding as needed). The trained model processes sequences in batches, generating two logits $[z_0, z_1]$ for each read corresponding to biological and artificial chimeric classes. Classification is determined by $\hat{y} = \text{argmax}(z_0, z_1)$. ChimeraLM outputs a filtered BAM file containing only reads classified as biological, which can be directly used for downstream analyses including SV calling.

Performance evaluation

Test set evaluation

Final model performance was evaluated on the held-out test set and the independent MinION Mk1c dataset. Metrics (precision, recall, and F1 score) were computed as described in the training section, where true positives represent chimeric reads correctly classified as artificial and true negatives represent biological reads correctly classified as biological.

SV calling

SVs were called using multiple tools to ensure comprehensive detection. For long-read data (ONT PromethION P2 and MinION Mk1c), we used Sniffles v2.5 [14, 15], DeBreak v1.2 [16], SVIM v2.0.0 [17], and cuteSV v2.1.1 [18]. For short-read data of the PC3 cell line, we used both the CCLE Illumina WGS dataset and the PRJNA361315

Illumina WGS dataset, processed with Manta v1.6.0 [48], DELLY v1.5.0 [49], and SvABA v1.1.0 [50]. All tools were executed with default recommended parameters.

Gold standard SV dataset construction

To evaluate the impact of ChimeraLM on SV detection accuracy, we generated a high-confidence gold-standard SV set from bulk PC3 sequencing data. All SV comparisons and breakpoint corrections were performed using OctopuSV v0.2.3 [51]. Four bulk datasets were integrated: ONT MinION Mk1c, ONT PromethION P2, the CCLE Illumina WGS dataset, and the PRJNA361315 Illumina WGS dataset. SVs were called independently within each dataset, and events supported by at least two SV callers were retained. The remaining calls were then compared across datasets, and SVs observed in at least two of the four datasets were designated as gold-standard events for benchmarking.

SV benchmarking analysis

To assess the impact of ChimeraLM on SV calling accuracy, we compared SV calls from unfiltered WGA data and ChimeraLM-filtered WGA data against two references: (1) the stringent multi-platform gold standard dataset, and (2) platform-matched long-read bulk sequencing data. Benchmarking was performed using Truvari v4.2.2 [52] with default parameters. SVs were considered supported if they matched reference variants within the defined breakpoint tolerance. Validation rates were calculated as the proportion of called SVs supported by the reference. This dual benchmarking strategy quantifies both improvements in detecting high-confidence multi-platform SVs and the retention of platform-specific true variants.

Benchmarking against existing methods

ChimeraLM was compared to existing computational methods for detecting amplification-induced chimeric artifacts: SACRA [25] (GitHub commit 9a2607e), 3rd-ChimeraMiner [13] (GitHub commit 04b5233), and CADECT v1.2 [11]. Both tools were applied to WGA data from PromethION P2 and MinION Mk1c platforms using default parameters as recommended in their documentation. Performance was evaluated by measuring the percentage reduction in chimeric reads relative to unprocessed WGA data. Chimeric reads were identified using WGA tag-based alignment criteria (reads with SA tags indicating split alignments), and reduction rates were calculated as the proportion of chimeric reads removed by each method.

Attention weight analysis

To investigate ChimeraLM's interpretability, we analyzed attention weights from the pooling mechanism for representative chimeric reads. Attention weights indicate the relative importance assigned to each sequence position during classification. For selected reads, we extracted per-position attention weights and visualized them alongside read alignments to identify whether the model focuses on mechanistically relevant regions.

Chimeric junction positions were identified from alignment data (defined by breakpoints in SA tags). A region of ±50 bp surrounding each junction was designated as the junction region. Attention weights within junction region were compared to non-junction regions using the Wilcoxon rank-sum test [53], with statistical significance assessed at $p < 0.001$.

Data visualization

Figures were generated using Python with Matplotlib [54] and Seaborn [55].

Computing resources

Computations were performed on a high performance computing (HPC) server with 64-core Intel Xeon Gold 6338 CPU, 256 GB RAM, and two NVIDIA A100 GPUs (80 GB memory each).

Extended Data Table 1 Sequencing and alignment statistics of PC3

Sample	Platform	Reads ($\times 10^6$)	Total bases (Gb)	Total bases aligned (Gb)	Fraction aligned	Mean length (bp)	Mean quality (Q)	Average identity (%)
WGA	MinION	9.11	14.6	10.4	0.7	1,603	14.3	97.6
WGA	PromethION	44.69	128.2	69.2	0.5	2,869	14.5	96.1
Bulk	MinION	0.97	8.1	7.1	0.9	8,310	17.2	97.3
Bulk	PromethION	8.00	69.9	62.4	0.9	8,732	18.5	97.7

Supplementary information.

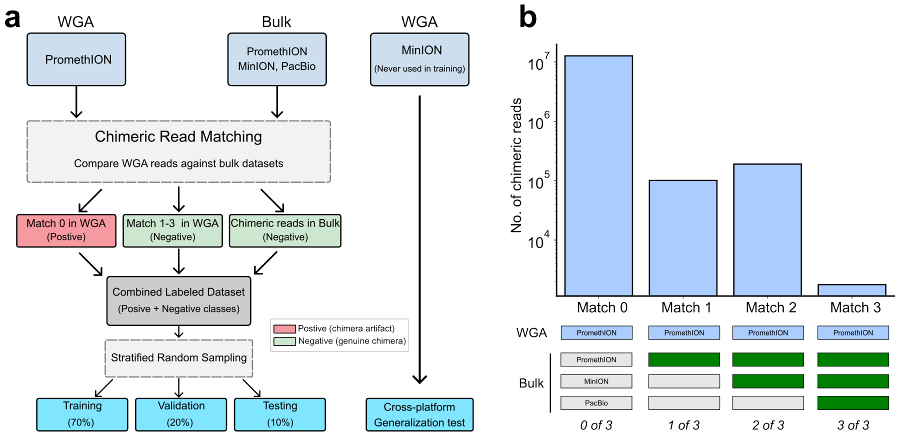

Extended Data Fig. 1 Training dataset construction and bulk-supported labeling strategy. (a) Workflow for generating labeled training data. WGA PromethION data is compared against three independent bulk sequencing datasets (PromethION, MinION, and PacBio). Reads with no bulk matches (Match 0) are labeled artificial; reads matching one or more bulk datasets (Match 1–3) are labeled biological, along with chimeric reads sampled directly from bulk data. The labeled dataset is split into training (70%), validation (20%), and test (10%) sets. The WGA MinION dataset is reserved for independent cross-platform evaluation. **(b)** Distribution of chimeric read matches. Bar chart shows the number of WGA PromethION chimeric reads (log scale) by bulk dataset matches. Match 0 reads (∼10^7) lacking bulk validation are classified as artificial; Match 1–3 reads with bulk support are classified as biological. The substantial imbalance reflects high prevalence of WGA-induced artifacts.

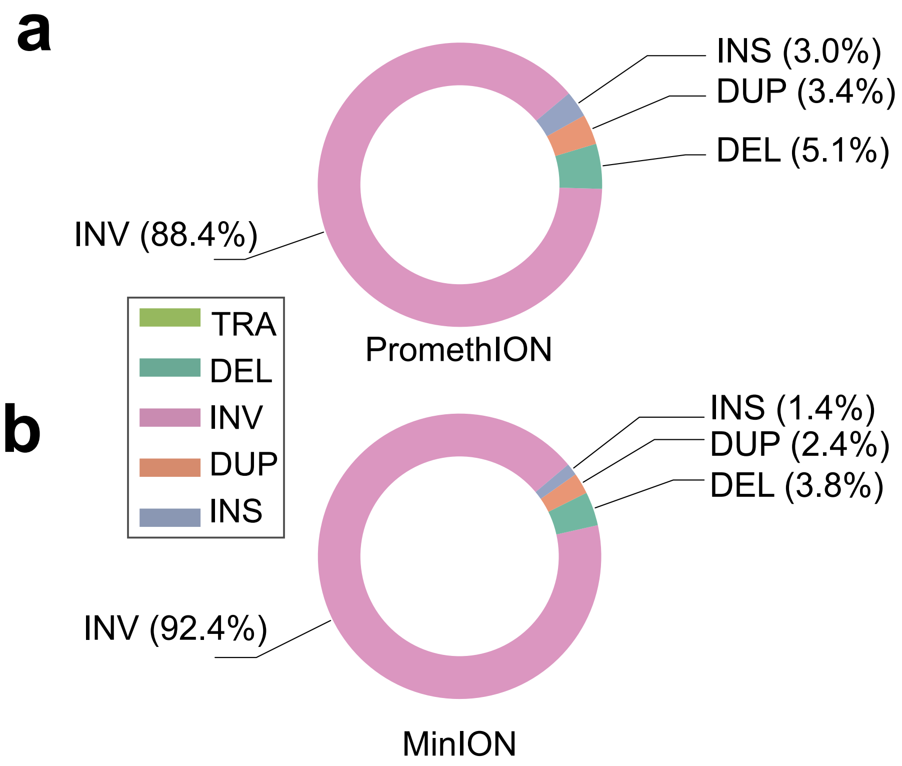

Extended Data Fig. 2 Composition of artifact-supported SVs for PromethION (a) and MinION (b). Donut charts summarize the distribution of SV types including translocation (TRA), deletion (DEL), inversion (INV), duplication (DUP), and insertion (INS) among events supported exclusively by chimera artifacts, representing artificial SVs preferentially removed by ChimeraLM.

Acknowledgements. We thank Tingyou Wang for guidance on figure preparation. This project was supported in part by NIH grants R35GM142441 and R01CA259388 awarded to RY.

Declarations

Author Contributions. YL, QG and RY designed the study. YL and QG performed the analysis. QG performed the experiments. YL and QG designed and implemented the model. YL built the command-line tool and documentation. YL, QG and RY wrote the manuscript. RY supervised this work.

Data Availability. The raw sequencing data generated in this study have been deposited in the NCBI Sequence Read Archive (SRA) under BioProject accession PRJNA1354861. The dataset includes Oxford Nanopore long-read whole-genome sequencing of PC3 prostate cancer cells and MDA-amplified single-cell derivatives. The individual SRA accessions are as follows: PC3 bulk (MinION Mk1C), SRR35904028; PC3 bulk (PromethION P2), SRR35904029; PC3 10-cell WGA (MinION Mk1C), SRR35904026; PC3 10-cell WGA (PromethION P2), SRR35904027. We can access the data at the following link: https://dataview.ncbi.nlm.nih.gov/object/PRJNA1354861?reviewer=viej6cv6mgbli3n7a9a5k1bsb3

Code Availability. ChimeraLM, implemented in Python, is open source and available on GitHub (https://github.com/ylab-hi/ChimeraLM) under the Apache License, Version 2.0. The package can be installed via PyPI (https://pypi.org/project/chimeralm) using pip, with wheel distributions provided for Windows, Linux, and macOS to ensure easy cross-platform installation. An interactive demo is available on Hugging Face (https://huggingface.co/spaces/yangliz5/ChimeraLM), allowing users to test ChimeraLM's functionality without local installation. For large-scale analyses, we recommend using ChimeraLM on systems with GPU acceleration. Detailed system requirements and optimization guidelines are available in the repository's documentation (https://ylab-hi.github.io/ChimeraLM/).

Conflict of interest. The authors declare no competing interests.

Acronyms

CPU central processing unit 12

DEL deletion 7, 21

dMDA droplet-based MDA 12

DUP duplication 7, 21

GLM genomic language model 1, 2, 12

GPU graphics processing unit 12, 16, 19, 22

HPC high performance computing 19

INS insertion 7, 21

INV inversion 7, 21

LIANTI linear amplification via transposon insertion 12

MALBAC multiple annealing and looping-based amplification cycles 12

MDA multiple displacement amplification 2, 9

MLP multilayer perceptron 4, 5, 15, 16

ONT Oxford Nanopore Technologies 3, 7, 8, 11, 13, 14, 17, 18

PacBio Pacific Biosciences 3, 14

PTA primary template-directed amplification 12

SA supplementary alignment 13, 14, 17–19

SV structural variation 1–4, 6–9, 11, 12, 14, 17, 18, 21

TRA translocation 7, 21

WGA whole genome amplification 1–12, 14, 17–20

WGS whole genome sequencing 7, 8, 17, 18

References

[1] Kalef-Ezra, E. *et al.* Single-cell somatic copy number variants in brain using different amplification methods and reference genomes. *Communications Biology* 1288 (2024).

[2] Navin, N. *et al.* Tumour evolution inferred by single-cell sequencing. *Nature* **472**, 90–94 (2011).

[3] Sun, C. *et al.* Mapping recurrent mosaic copy number variation in human neurons. *Nature Communications* 4220 (2024).

[4] Gawad, C., Koh, W. & Quake, S. R. Single-cell genome sequencing: current state of the science. *Nature Reviews Genetics* 175–188 (2016).

[5] Chen, C. *et al.* Single-cell whole-genome analyses by linear amplification via transposon insertion (LIANTI). *Science (new York, N.Y.)* **356**, 189–194 (2017).

[6] Macaulay, I. C. & Voet, T. Single cell genomics: Advances and future perspectives. *PLOS Genetics* **10**, e1004126 (2014).

[7] de Bourcy, C. F. A. *et al.* A quantitative comparison of single-cell whole genome amplification methods. *PLoS ONE* e105585 (2014).

[8] Biezuner, T. *et al.* Comparison of seven single cell whole genome amplification commercial kits using targeted sequencing. *Scientific Reports* 17171 (2021).

[9] Lu, N., Qiao, Y., Lu, Z. & Tu, J. Chimera: The spoiler in multiple displacement amplification. *Computational and Structural Biotechnology Journal* 1688–1696 (2023).

[10] Lasken, R. S. & Stockwell, T. B. Mechanism of chimera formation during the multiple displacement amplification reaction. *BMC Biotechnology* **7**, 19 (2007).

[11] Agyabeng-Dadzie, F. *et al.* Evaluating the benefits and limits of multiple displacement amplification with whole-genome oxford nanopore sequencing. *Molecular Ecology Resources* e14094 (2025).

[12] Dean, F. B. *et al.* Comprehensive human genome amplification using multiple displacement amplification. *Proceedings of the National Academy of Sciences* **99**, 5261–5266 (2002).

[13] Lu, N. *et al.* Exploration of whole genome amplification generated chimeric sequences in long-read sequencing data. *Briefings in Bioinformatics* **24**, bbad275 (2023).

[14] Sedlazeck, F. J. *et al.* Accurate detection of complex structural variations using single-molecule sequencing. *Nature Methods* 461–468 (2018).

[15] Smolka, M. *et al.* Detection of mosaic and population-level structural variants with sniffles2. *Nature Biotechnology* 1571–1580 (2024).

[16] Chen, Y. *et al.* Deciphering the exact breakpoints of structural variations using long sequencing reads with DeBreak. *Nature Communications* 283 (2023).

[17] Heller, D. & Vingron, M. SVIM: Structural variant identification using mapped long reads. *Bioinformatics* 2907–2915 (2019).

[18] Jiang, T. *et al.* Long-read-based human genomic structural variation detection with cuteSV. *Genome Biology* 189 (2020).

[19] Gonzalez-Pena, V. *et al.* Accurate genomic variant detection in single cells with primary template-directed amplification. *Proceedings of the National Academy of Sciences* **118**, e2024176118 (2021).

[20] Kosugi, S. *et al.* Comprehensive evaluation of structural variation detection algorithms for whole genome sequencing. *Genome Biology* **20**, 117 (2019).

[21] Alkan, C., Coe, B. P. & Eichler, E. E. Genome structural variation discovery and genotyping. *Nature Reviews Genetics* **12**, 363–376 (2011).

[22] Hård, J. *et al.* Long-read whole-genome analysis of human single cells. *Nature Communications* **14**, 5164 (2023).

[23] Gupta, P., O'Neill, H., Wolvetang, E. J., Chatterjee, A. & Gupta, I. Advances in single-cell long-read sequencing technologies. *NAR Genomics and Bioinformatics* **6**, lqae047 (2024).

[24] Wen, L. & Tang, F. Single-cell omics sequencing technologies: The long-read generation. *Trends in Genetics* **0** (2025).

[25] Kiguchi, Y., Nishijima, S., Kumar, N., Hattori, M. & Suda, W. Long-read metagenomics of multiple displacement amplified DNA of low-biomass human gut phageomes by SACRA pre-processing chimeric reads. *DNA Research* **28**, dsab019 (2021).

[26] Ha, Y.-J. *et al.* Comprehensive benchmarking and guidelines of mosaic variant calling strategies. *Nature Methods* **20**, 2058–2067 (2023).

[27] Höijer, I. *et al.* Amplification-free long-read sequencing reveals unforeseen CRISPR-Cas9 off-target activity. *Genome Biology* **21**, 290 (2020).

[28] Li, Y. *et al.* A genomic language model for chimera artifact detection in nanopore direct rna sequencing. *bioRxiv* (2024). URL https://www.biorxiv.org/content/early/2024/10/25/2024.10.23.619929.

[29] Nguyen, E. *et al.* *HyenaDNA: Long-range genomic sequence modeling at single nucleotide resolution*, Vol. 36, 43177–43201 (Curran Associates, Inc., 2023).

[30] Dalla-Torre, H. *et al.* Nucleotide transformer: building and evaluating robust foundation models for human genomics. *Nature Methods* 287–297 (2025).

[31] Zhou, Z. *et al.* *DNABERT-2: Efficient foundation model and benchmark for multi-species genomes*, 1–24 (OpenReview.net, 2024).

[32] Consens, M. E. *et al.* To transformers and beyond: Large language models for the genome (2023). arXiv:2311.07621.

[33] Poli, M. *et al.* *Hyena hierarchy: Towards larger convolutional language models*, Vol. 202, 28043–28078 (PMLR, 2023).

[34] Barretina, J. *et al.* The Cancer Cell Line Encyclopedia enables predictive modelling of anticancer drug sensitivity. *Nature* **483**, 603–607 (2012).

[35] Seim, I., Jeffery, P. L., Thomas, P. B., Nelson, C. C. & Chopin, L. K. Whole-Genome Sequence of the Metastatic PC3 and LNCaP Human Prostate Cancer Cell Lines. *G3 (Bethesda, Md.)* **7**, 1731–1741 (2017).

[36] Mahmoud, M. *et al.* Structural variant calling: The long and the short of it. *Genome Biology* **20**, 246 (2019).

[37] Zong, C., Lu, S., Chapman, A. R. & Xie, X. S. Genome-wide detection of single-nucleotide and copy-number variations of a single human cell. *Science* 1622–1626 (2012).

[38] Dippenaar, A. *et al.* Droplet based whole genome amplification for sequencing minute amounts of purified mycobacterium tuberculosis DNA. *Scientific Reports* **14**, 9931 (2024).

[39] PLC., O. N. Dorado. https://github.com/nanoporetech/dorado (2023).

[40] Martin, M. Cutadapt removes adapter sequences from high-throughput sequencing reads. *Embnet.journal* **17**, 10–12 (2011).

[41] Li, H. Minimap2: Pairwise alignment for nucleotide sequences. *Bioinformatics* 3094–3100 (2018).

[42] Danecek, P. *et al.* Twelve years of SAMtools and BCFtools. *GigaScience* giab008 (2021).

[43] De Coster, W. & Rademakers, R. NanoPack2: Population-scale evaluation of long-read sequencing data. *Bioinformatics* **39**, btad311 (2023).

[44] Paszke, A. *et al. PyTorch: An imperative style, high-performance deep learning library*, Vol. 32, 8024–8035 (Curran Associates, Inc., 2019).

[45] Falcon, W. & The PyTorch Lightning team. PyTorch Lightning. GitHub repository (2019). URL https://github.com/Lightning-AI/lightning.

[46] Loshchilov, I. & Hutter, F. *Decoupled weight decay regularization* (2019).

[47] Yadan, O. Hydra - a framework for elegantly configuring complex applications. GitHub repository (2019). URL https://github.com/facebookresearch/hydra.

[48] Chen, X. *et al.* Manta: Rapid detection of structural variants and indels for germline and cancer sequencing applications. *Bioinformatics* 1220–1222 (2016).

[49] Rausch, T. *et al.* DELLY: Structural variant discovery by integrated paired-end and split-read analysis. *Bioinformatics* i333–i339 (2012).

[50] Wala, J. A. *et al.* SvABA: Genome-wide detection of structural variants and indels by local assembly. *Genome Research* 581–591 (2018).

[51] Guo, Q., Li, Y., Wang, T.-Y., Ramakrishnan, A. & Yang, R. OctopuSV and TentacleSV: A one-stop toolkit for multi-sample, cross-platform structural variant comparison and analysis. *Bioinformatics* btaf599 (2025).

[52] English, A. C., Menon, V. K., Gibbs, R. A., Metcalf, G. A. & Sedlazeck, F. J. Truvari: Refined structural variant comparison preserves allelic diversity. *Genome*

Biology **23**, 271 (2022).

[53] Virtanen, P. *et al.* SciPy 1.0: Fundamental algorithms for scientific computing in python. *Nature Methods* 261–272 (2020).

[54] Hunter, J. D. Matplotlib: A 2d graphics environment. *Computing in Science & Engineering* 90–95 (2007).

[55] Waskom, M. L. seaborn: statistical data visualization. *Journal of Open Source Software* 3021 (2021).